Food Chemistry 421 (2023) 136152

Contents lists available at ScienceDirect

Food Chemistry

journal homepage: www.elsevier.com/locate/foodchem

A novel polysaccharide from *Rubus chingii* Hu unripe fruits: Extraction optimization, structural characterization and amelioration of colonic inflammation and oxidative stress

Hanqi Luo [a], Na Ying [a], Qihui Zhao [a], Junli Chen [a], Hangying Xu [a], Wu Jiang [b], Yaozong Wu [c], Yinliang Wu [c], Hongchang Gao [a,*], Hong Zheng [a,*]

[a] School of Pharmaceutical Sciences, Wenzhou Medical University, Wenzhou 325035, China
[b] Zhejiang Institute of Subtropical Crops, Zhejiang Academy of Agricultural Sciences, Wenzhou 325005, China
[c] Jiangsu Sanshu Biotechnology Co., Ltd., Nantong 226006, China

ARTICLE INFO

Keywords:
Raspberry
Polysaccharide
Colon
Inflammation
Gut microbiota

ABSTRACT

Raspberry is used as a medicine food homology species and its polysaccharides are worthy being investigated and developed. In the present study, a novel polysaccharide of unripe raspberry fruits (pRCP) was extracted and characterized. The results show that pRCP was an acidic heteropolysaccharide and its Mw value was 74.86 kDa with a high homogeneity. The main chain of pRCP consisted of → 3,6)-*β*-Gal*p*(1 → and → 5)-*α*-Ara*f*(1→, and its side chain was composed of *α*-Ara*f*(1 → linked to the C3 position of → 3,6)-*β*-Gal*p*(1 →. In addition, pRCP supplementation increased the gut microbial diversity and reduced harmful bacteria including *Erysipelatoclostridium* and *Negativibacillus* in high-fat diet (HFD)-fed mice. Treatment with pRCP also alleviated HFD-induced colonic inflammation and oxidative stress in mice. These beneficial effects can be transferred to recipient mice by faecal microbiota transplantation from pRCP-treated mice. Therefore, our study suggests that pRCP could be used as a potential prebiotics to improve intestinal health by modulating the gut microbiota.

1. Introduction

Raspberry (*Rubus chingii* Hu.) is widely cultivated in the world, especially in Asia, Europe and North America (Burton-Freeman et al., 2016). In China, raspberry has been defined as a medicine food homology species due to its nutritional and medicinal ingredients (Mazur et al., 2014). Ripe raspberries are commonly harvested as edible fruits and have beneficial effects on oxidative damage, inflammation, hyperglycemia and dyslipidemias (Noratto et al., 2017; Lu et al., 2022). Of note, immature fruits are also utilized as a folk medicine to treat diarrhea, wounds and colic (Staszowska-Karkut & Materska, 2020). Relative to ripe fruits, however, the novel constituent and function of unripe raspberries still need to be further discovered for the health-promoting effect.

The main functional elements in raspberry fruits include phenolics, flavonoids, triterpenes, minerals, vitamins, carotenoids and organic acids (Mazur et al., 2014). Noratto et al. (2017) reported that raspberry polyphenolics can alleviate oxidative stress in obese diabetic mice. Phenolic/anthocyanin-rich fractions are one of the major ingredients for antioxidant and anti-inflammatory properties of raspberry fruits (Szymanowska et al., 2018). Moreover, raspberry ellagitannins have been revealed to exhibit an antimycotic effect (Klewicka et al., 2020). Noteworthily, polysaccharides from medicine and food homology materials are also attracting great interest because of their health-promoting properties for immunomodulation (Chen & Huang, 2018), diabetes (Zhou et al., 2020) and obesity (Su et al., 2021a). Yu et al. (2015) extracted a water-soluble polysaccharide from raspberry fruits and reported its antioxidant and non-enzymatic glycation inhibitory ability. In addition, raspberry polysaccharides have also been shown to exert α-amylase inhibitory capacity (Xu et al., 2019) and macrophage activation activity (Yang et al., 2022). Currently, however, there are still few studies regarding the structure and function of polysaccharides from unripe raspberry fruits, which are generally used in traditional Chinese medicine.

Nowadays, the excessive consumption of high-fat diet (HFD) is becoming one of the major causes for human diseases including obesity (Ravussin & Tataranni, 1997), non-alcoholic fatty liver disease (Lian et al., 2020) and diabetes (Hancock et al., 2008). Long-term HFD intake

* Corresponding authors.
E-mail addresses: gaohc27@wmu.edu.cn (H. Gao), 123zhenghong321@163.com (H. Zheng).

https://doi.org/10.1016/j.foodchem.2023.136152
Received 21 December 2022; Received in revised form 19 March 2023; Accepted 11 April 2023
Available online 18 April 2023
0308-8146/© 2023 Elsevier Ltd. All rights reserved.

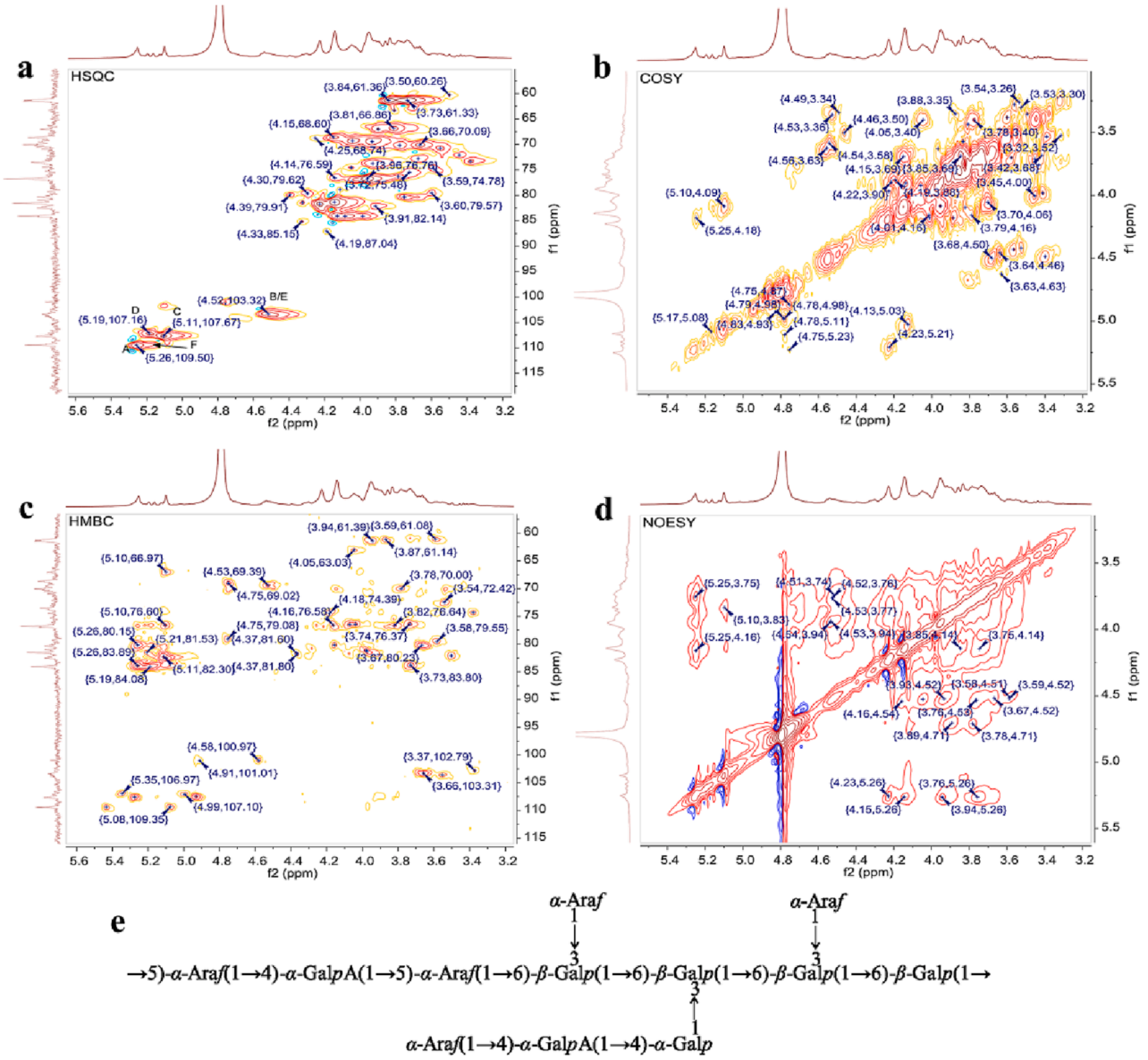

Fig. 1. Structural characterization of raspberry polysaccharide. (a-d) Typical 2D NMR spectra including (a) HSQC, (b) COSY, (c) HMBC and (d) NOESY; (e) The detailed structure of raspberry polysaccharide.

has been also reported to affect the gut microbiota and intestinal health (Rohr et al., 2020). We hypothesized that raspberry polysaccharides have the ability to maintain intestinal homeostasis by modulating the gut microbiota. In this study, therefore, we first optimized the extraction procedure of polysaccharides from unripe raspberry fruits by using a three steps methodology and characterized the detailed structure of the main fraction of polysaccharides (pRCP) via monosaccharide analysis, FT-IR, molecular weight distribution and homogeneity analysis, methylation analysis and 1D/2D NMR. Subsequently, we treated HFD-fed mice with intragastric administration of pRCP for 12 weeks and examined its effects on the gut microbiota and colonic inflammation and oxidative stress. Finally, the faecal microbiota from pRCP-treated mice was transferred to HFD-fed recipient mice to confirm the causal role of the gut microbiota in the protective effect of pRCP on intestinal health. Our results are expected to provide a novel polysaccharide from unripe raspberry fruits and its potential application as a prebiotics for improving gut homeostasis.

2. Materials and methods

2.1. Raspberry materials

Raspberry fruits (*Rubus chingii* Hu.) were harvested in mid-May from a planting farm at Hangzhou city (Zhejiang, China). The fruits were washed with distilled water and dried to constant weight at 50 °C. The dried fruits were pulverized by using a stainless steel pulverizer (LFP-8007, Yongkang Ruideshan Electromechanical Co., Ltd.) and passed through a 60-mesh sieve. Subsequently, the raspberry powder was soaked at room temperature for 2 h in 80% ethanol to remove plant pigments, dried at 50 °C to constant weight and kept in a vacuum drying desiccator until use.

2.2. Optimal extraction of raspberry crude polysaccharide

Raspberry crude polysaccharide (RCP) was extracted using the water-extraction and alcohol-precipitation method, as illustrated in Fig. S1a. First, we used three different methods to pretreat the dried

raspberry powder: M1, the sample was soaked in distilled water (1:3, w/v) for 30 min; M2, the sample was soaked in 50% ethanol (1:3, w/v) for 30 min; M3, the sample was soaked in 50% ethanol (1:3, w/v) for 30 min and then ultrasonicated for 10 min. The pretreated sample was extracted in distilled water (1:20, w/v) at 80 °C for 1 h and centrifuged at 3,000 g for 10 min. The supernatant was collected and concentrated to 1/4 of the original volume with a vacuum rotary evaporator at 42 °C. For ethanol precipitation, a 4-fold volume of 95% ethanol was added and stood at 4 °C for 12 h, and then centrifuged at 3,000 g for 10 min. The precipitate was dissolved in distilled water and treated with Sevage reagent (chloroform/*n*-butanol, 4:1, v/v) to remove proteins. Finally, the extract solution was lyophilized by vacuum freeze-drying to obtain RCP.

In this study, the pretreatment parameters of raspberry were further optimized to maximize the extraction yield of RCP using Design-Expert software (v13, Stat-Ease, Minneapolis, USA). The multivariate optimization was carried out by three steps: (i) screening of the significant parameters by Plackett-Burman design; (ii) determination of the neighborhood of the optimum by steepest ascent experiment; (iii) optimization of the significant parameters by Box-Behnken design.

2.3. Isolation and purification of RCP

RCP solution (20 mg/mL) was prepared in deionized water and then loaded on the chromatography column containing DEAE seplife FF (Sunresin, Xi'an, China). The column was eluted with NaCl solution (0.00–0.30 M) to obtain four fractions (RCP1, RCP2, RCP3 and RCP4). The main fraction (RCP1) was then filtered with 3000 Da dialysis bag to desalt and loaded on a Sephacryl S-400HR column (GE Healthcare, Piscataway, USA) with distilled water at a flow rate of 0.5 mL/min to collect the pure RCP (pRCP). In this study, each eluate was collected into one tube and total carbohydrate content was detected with glucose as a standard by the anthrone-sulfonic acid method. Finally, the pRCP sample was obtained after vacuum freeze-drying.

2.4. Analysis of monosaccharide and uronic acid compositions in pRCP

The monosaccharide and uronic acid compositions of pRCP were determined by using the published method (Salvador et al., 2000) with a minor modification. In brief, approximately 5 mg of pRCP powder was weighed into a sealed tube and hydrolyzed with 1 mL of trifluoroacetic acid (TFA, 2.0 M) for 2 h at 121 °C and dried with nitrogen. pRCP hydrolysates were washed three times with methanol and dried with nitrogen. Then, the dried hydrolysates were redissolved in sterile water and filtered through 0.22 μm microporous filtering film into a sample tube for analysis. The monosaccharide and uronic acid compositions were analyzed by high-performance anion-exchange chromatography on a CarboPac PA-20 anion-exchange column (Dionex, 3 × 150 mm) equipped with a pulsed amperometric detector (PAD, Dionex ICS5000 system). Data were acquired on Ion Chromatography System 5000 (ICS5000, Thermo Scientific) and processed using Chromeleon 7.2 CDS (Thermo Scientific). The absolute quantification was carried out by using external standards including nine neutral monosaccharides (fucose, arabinose, rhamnose, galactose, glucose, xylose, mannose, fructose and ribose) and four uronic acids (galacturonic acid, guluronic acid, mannuronic acid and glucuronic acid).

2.5. Fourier transform-infrared (FT-IR) analysis

The infrared spectrum of pRCP was recorded with a Nicolet iZ-10 FT-IR instrument (Thermo Fisher Scientific) in the range of 4000–400 cm^{-1}. In brief, the dried pRCP (2 mg) and KBr (200 mg) were weighed and pressed into tablets for FT-IR analysis, and KBr tablet was used as a blank control.

2.6. Molecular weight and homogeneity

The pRCP sample were dissolved in $NaNO_3$ aqueous solution (0.1 M) containing 0.02% NaN_3 at the concentration of 1 mg/mL and filtered through a filter of 0.45 μm pore size. The homogeneity, molecular weight and root mean square (RMS) radius of various pRCP fractions were analyzed by the *SEC*-MALLS-RI. The weight- and number-average molecular weight (Mw and Mn) and polydispersity index (Mw/Mn) were measured on a DAWN HELEOS-II laser photometer (He-Ne laser, λ = 663.7 nm, Wyatt Technology Co., Santa Barbara, USA) equipped with three tandem columns (300 × 8 mm, Shodex OH-pak SB-805, 804 and 803; Showa Denko K.K., Tokyo, Japan) at 45℃ using a model column heater. The mobile phase was 0.1 M $NaNO_3$ solution containing 0.02% NaN_3 and the flow rate is 0.4 mL/min. The concentration and the dn/dc value of the fractions were simultaneously analyzed with a differential refractive index detector (Optilab *T*-rEX, Wyatt Technology Co., Santa Barbara, CA, USA). In this study, the dn/dc value of the fractions in 0.1 M $NaNO_3$ aqueous solution containing 0.02% NaN_3 was determined to be 0.141 mL/g. Data were acquired and processed by using ASTRA6.1 (Wyatt Technology). The slope in the conformation plot based on molar mass and RMS radius was calculated as a reference for the molecular configuration (Zhang et al., 2020).

2.7. Nuclear magnetic resonance (NMR) analysis

The pRCP sample (10 mg) was dissolved into 0.5 mL of D_2O and transferred into an NMR tube. Then, the one-dimension (^1H and ^{13}C) and two-dimension (COSY, HSQC, HMBC and NOESY) NMR spectra were acquired by a Bruker 500 MHz NMR spectrometer (Brucker, Rheinstetten, Germany) equipped with a 5 mm quadruple probe head QXI ($^1H/^{31}P/^{13}C/^{15}N$) at 25 °C. Data was analyzed using MestRe Nova 5.3.0 software (Mestrelab Research S.l.).

2.8. Methylation analysis

In this study, we used the carboxyl reduction method based on Kim and Carpita (1992) to reduce uronic acid and its derivatives prior to the methylation analysis. In this method, carboxylic esters are first reduced with sodium borodeuteride ($NaBD_4$) to produce 6,6′-dideuterio-sugars, which can be separated from neutral sugars on GC–MS by the presence of fragment ions with increased masses (M + 2). Specifically, the polysaccharide pRCP sample was reduced with $NaBH_4$ and $NaBD_4$, dialyzed and lyophilized to acquire the reduzates and then methylated in DMSO/NaOH with CH_3I. These procedures were performed three times to ensure complete pRCP methylation. Then, trifluoroacetic acid (TFA, 2 M) was added to the methylated polysaccharide and reacted for 90 min at 121 °C. The sample was reduced with $NaBH_4$ (1 M) at room temperature overnight and acetylated by acetic anhydride. Afterward, the sample was extracted with dichloromethane and the organic phase was dried with nitrogen for GC–MS analysis. The extracts were analyzed by GC–MS (7890A-5977B, Agilent, California, USA) equipped with a BPX-70 column (30 m × 0.25 mm × 0.25 μm). The injection volume was 1 μL with a split ratio of 10:1 and the injection temperature was 260 °C. High purity helium was used as the carrier gas at a flow rate of 1.0 mL/min. The column temperature started with 140 °C for 2 min, increased to 230 °C at a rate of 3 °C/min and held for 3 min. Mass spectra were recorded with an electron impact ion source (EI) and a MassHunter workstation within 30–600 *m/z* and energy of ionization was 70 eV.

2.9. Scanning electron microscopy

The morphology of pRCP was examined with high-resolution field emission scanning electron microscope (Hitachi, Regulus 8100, Japan). In brief, pRCP was sieved with a 100-mesh sieve, coated with a thin gold layer and observed at an accelerating voltage of 15.0 kV under high vacuum.

2.10. Animal experiment

Male 6-week-old C57BL/6 mice with body weight of 18–22 g were purchased from the Vital River Laboratory Animal Technology (Beijing, China). All mice were housed in specific-pathogen-free (SPF) colony under a fully controlled environment (temperature: 22 ± 2℃; humidity: 45 ± 3%; light/dark cycle: 12/12 h) at the Laboratory Animal Center of Wenzhou Medical University (WMU, Wenzhou, China). Mice were freely given standard chow and tap water during the experimental period. All animal care and procedures were performed according to the Guide for the Care and Use of Laboratory Animals and approved by the Institutional Animal Care and Use Committee of WMU (No.: xmsq2022-0670).

After a 1-week acclimatization, all mice were randomly assigned into three groups (n = 9 for each group): Chow, mice fed with normal chow (16.7 % kcal from fat, 19.3 % kcal from protein, and 63 % kcal from carbohydrate); HFD, mice fed with high-fat diet (60 % kcal from fat, 20 % kcal from protein, and 20 % kcal from carbohydrate); pRCP, mice fed with HFD plus daily administration of pRCP solution prepared in sterile water (0.25 g/mL, w/v) at a dose of 0.1 g/kg body weight by gavage at 9:00 a.m. for 12 weeks. The body weight of mice was recorded biweekly by using an electronic balance.

2.11. Faecal microbiota transplantation

Mice were given HFD for 12 weeks and randomly assigned into two groups (n = 9 for each group): HFD-R, mice receiving the faecal microbiota from mice fed with HFD; pRCP-R, mice receiving the faecal microbiota from mice fed with pRCP. To deplete the indigenous gut flora, recipient mice were treated with an antibiotic cocktail containing vancomycin (50 mg/kg), neomycin (100 mg/kg), metronidazole (100 mg/kg) and amphotericin B (1 mg/kg) by gavage once a day and with drinking water containing ampicillin (1 g/L) for 7 days. Antibiotics used herein were purchased from the Meilun Biotech Company (Dalian, China). Fresh faecal pellets from the donor mice was rapidly collected after defecation every morning and resuspended in sterile PBS buffer (7.5 mL/g feces, v/w). The mixture was vortexed vigorously for 2 min and then centrifuged at 1,000 g for 5 min at 4 °C to remove particles. Afterward, 100 μL of the bacterial suspension was transplanted to HFD-fed recipient mice by gavage once a day for 2 weeks.

2.12. Sample collection

In this study, fresh faecal pellets of mice were promptly collected after defecation into sterile tubes every morning. Mice were anaesthetized with isoflurane and sacrificed by rapid decapitation, and then the colonic tissue sample was rapidly dissected and frozen in liquid nitrogen. All samples were kept at −80 °C until use.

2.13. 16S rRNA sequencing analysis

Total microbial DNA was extracted by using the TIANamp stool DNA kit in line with the manufacturer's instruction (TianGen, China). The agarose gel electrophoresis (AGE, 1%) was used to determine the purity of total DNA. In the present study, the V3-V4 region in 16S rRNA gene was amplified with the universal primers including 515F (5′-GTG CCA GCM GCC GCG GTA A-3′) and 806R (5′-GGA CTA CHV GGG TWT CTA AT-3′). Next, the PCR product was purified with the QIAquick gel extraction kit according to the manufacturer's instruction (Qiagen, Germany) and sequenced by using an Illumina HiSeq2500 PE250 sequencer (San Diego, USA) at Novogene (Beijing, China).

The raw sequencing tags were filtered by merging paired-end reads in FLASH software (v1.2.7) and merged into the clean tags with QIIME2 software. The clean tags were produced by using UCHIME algorithm (v7.0.1001) and clustered to operational taxonomic units (OTUs) with a similarity cut-off of 97% under UPARSE pipeline (v7.0.1001). Then, the OTUs were annotated for taxonomic information at a confidence threshold of 80% using the Mothur method and SILVA database.

2.14. Immunohistochemical staining

In this study, mice (n = 3 per group) were anaesthetized with isoflurane and sacrificed by cardiac perfusion with normal saline. Then the colonic tissue samples were fixed in 4% paraformaldehyde in PBS buffer (0.1 M, pH = 7.5) for Immunohistochemical analysis. The colonic section was dewaxed using xylene, rehydrated in gradient alcohol, and incubated with the primary antibodies 8-OHDG (Abcam, ab48508, 1:200) and 4-HNE (Abcam, ab46545, 1:200) overnight at 4℃. After washing in PBS buffer for 3 times, the section was incubated with goat anti-mouse/rabbit IgG (H + L) secondary antibodies conjugated with horseradish peroxidase (HRP) for 1 h at 37℃ and stopped with DAB (3,3′-diaminobenzidine) chromogen kit (ZSGB-BIO, Beijing, China). The section was stained with hematoxylin, dehydrated with gradient ethanol and sealed with neutral gum. Finally, the image was taken using a Nikon ECLIPSE NI microscope (Nikon, Japan) and quantitatively processed by Image J software (v1.47, Bethesda, MD, USA).

2.15. Real-time qPCR analysis

Total RNA in colonic tissue samples was extracted using the Trizol reagent according to the manufacturer's instruction (Invitrogen, CA, USA). The purity of total RNA was determined by a NanoDrop spectrometer (Thermo Scientific, Wilmington, USA) and then reverse-transcribed to cDNA using the PrimeScript^{TM} RT Reagent Kit (TaKaRa, Kusatsu, Japan). The quantitative analysis was conducted under a 10 μL final reaction volume using SYBR Green PCR Master Mix (Bio-Rad, CA, USA) on a Bio-Rad CFX96 Real-Time PCR system (Bio-Rad, CA, USA). The mRNA expression level was calculated through the ΔΔCT method and GAPDH was used as an internal standard. In this study, specific primer pairs were synthesized at Sunny Biotechnology (Shanghai, China) as listed in Table S1.

2.16. Statistical analysis

In the present study, all mice were randomly assigned to experimental processes such as animal grouping and feeding, FMT, sample collection and data analysis. The gut microbiota data were log-transformed and Pareto-scaled, and then the differences of microbial patterns between different groups were analyzed using principal coordinate analysis (PCoA) with R software (v2.15.3). The statistical difference between two groups was evaluated by two-tailed unpaired student's T test. The statistical difference among different groups was analyzed using ANOVA with pairwise comparisons, and different lowercase letters in the figures represent a significant difference. The statistical difference in the number of observed species between different groups was assessed by using a repeated measure ANOVA. Analysis of difference of variables was carried out by SPSS 22.0 software (SPSS, Inc., Chicago, IL, USA) and a statistically significant was considered when $p < 0.05$. A volcano plot was performed by plotting $\log_2$ (FC, fold change) versus $-\log_{10}$ (p value) in R software (v2.15.3).

3. Results and discussion

3.1. Optimal extraction of RCP using a three steps methodology

The extraction flow diagram of raspberry crude polysaccharide (RCP) is shown in Fig. S1a. Sample pretreatment has been proven to play a key role in the extraction of bioactive compounds from plant materials (Ummat et al., 2021). In the present study, three different pretreatment methods were performed to extract RCP including water soak (M1), ethanol soak (M2) and ultrasonic-assisted ethanol soak (M3), as illustrated in Fig. S1a. The results demonstrate that M3 had a significantly higher extraction yield than M1 and M2 (Fig. S1b), suggesting that

Table 1
Yield and monosaccharide composition of raspberry polysaccharide.[a]

Parameter	Content (%)	
RCP1[b]	37.41 ± 1.2	
pRCP[c]	86.03 ± 2.5	
Carbohydrate	44.61 ± 0.7	
Protein	-[d]	
Monosaccharide	Content (μg/mg)	Proportion (%)
Fucose	1.91 ± 0.14	0.35
Arabinose	215.64 ± 10.98	39.76
Rhamnose	–	–
Galactose	213.84 ± 10.20	39.43
Glucose	11.72 ± 2.07	2.16
Xylose	8.32 ± 0.19	1.53
Mannose	13.91 ± 0.80	2.56
Fructose	–	–
Ribose	–	–
Galacturonic acid	46.44 ± 1.65	8.56
Guluronic acid	–	–
Glucuronic acid	30.60 ± 1.44	5.64
Mannuronic acid	–	–

[a] Data were expressed as Mean ± SD.
[b] The main fraction of raspberry polysaccharide.
[c] Pure raspberry polysaccharide.
[d] No detection.

ultrasonic-assisted method is an advantageous pretreatment for RCP extraction.

To further increase the extraction yield of RCP, herein we optimized seven key factors during ultrasonic-assisted pretreatment with a three steps methodology (Fig. S1c). First, a two-level Plackett-Burman design (PBD) was performed to select the important factors that significantly affect the extraction yield. The factors and their levels used in the PBD were listed in Table S2, and the changes in the extraction yield ranging from 3.98 ± 0.17 % to 5.78 ± 0.13 % were observed in the PBD (Table S3). The results from analysis of variance reveal that the regression model of the PBD was statistically significant (P = 0.0093, Table S4). Moreover, according to P values, the influence of each factor on the extraction yield was: X5 > X7 > X1 > X3 > X2 > X6 > X4. In this study, the top three factors, namely temperature (X5) and ultrasonic time (X7) during ultrasonic treatment and ethanol concentration (X1) during ethanol soak, were selected as the key factors to be further optimized for RCP extraction. Furthermore, the steepest ascent experiment was used to determine the neighborhood of the optimum (Hansen et al., 2019), and the Run 4 in Table S5 was selected as the center point. The Box-Behnken design (BBD) was formulated whose center point was moved in the direction of the condition giving the higher extraction yield (Table S6). Table S7 shows the extraction yield of RCP with different extraction conditions from the BBD. The ANOVA results from Table S8 reveal that the P value of the model was 0.0002 and the lack-of-fit was not statistically significant (P = 0.4891), indicating that the developed model was adequate. Besides, the coefficient of determination (R^2) of 0.9705 meant that there was a good correlation between the experimental values and the predicted values by the model, implying that the model had a high accuracy. Three-dimensional response surface plot was employed to provide a visual interaction between ethanol concentration and temperature (Fig. S1d), between ethanol concentration and ultrasonic time (Fig. S1e) and between temperature and ultrasonic time (Fig. S1f). By maximizing the extraction yield of RCP, the BBD model calculated the optimal values for these three factors and predicted the extraction yield of 8.34% (Table S9). Finally, the actual extraction yield of RCP was 8.30 ± 0.07% using the optimized method (Table S9), which is significantly higher than non-optimized extraction methods (Fig. S1b).

3.2. Isolation and purification of RCP

To further isolate and purify polysaccharides, RCP was separated into four fractions (RCP1, RCP2, RCP3 and RCP4) using a DEAE seplife FF cellulose chromatography column eluted with 0, 0.1, 0.2 and 0.3 M NaCl solutions (Fig. S2a). Then, the major fraction (RCP1, yield = 37.41%) was further purified with a Sephacryl S-400HR column to obtain the pure RCP (pRCP) with a yield of 86.03% (Fig. S2b; Table 1). The content of carbohydrates in pRCP was approximately 44.61% with glucose as a standard and the content of proteins was not detected (Table 1). Using the optimized method, approximately 2.67 g of pRCP can be obtained from 100 g of unripe raspberry fruits. Mazur et al. (2014) reported that the chemical compositions of red raspberry fruits were affected notably by genotype and harvest season. Excepting extraction methods, thus, we speculate that the yield of pRCP could be also dependent on the variety and ripeness of raspberries.

3.3. Physicochemical properties of pRCP

The chromatographic peaks of monosaccharide standards and pRCP hydrolysates are illustrated in Fig. S3a and S3b, respectively. The results reveal that pRCP was made up of fucose, arabinose, galactose, glucose, xylose, mannose, galacturonic acid and glucuronic acid. According to the quantitative results in Table 1, we found that arabinose and galactose were the main neutral monosaccharides with the proportion of 39.76% and 39.43%, respectively, suggesting that these two monosaccharides constructed the backbone sugar chain of pRCP. Similar results were obtained in other raspberry polysaccharides extracted by Chen et al. (2020) and Su et al. (2021b). In addition, the proportions of galacturonic acid and glucuronic acid were 8.56% and 5.64% in pRCP, respectively (Table 1), indicating that pRCP belongs to an acidic polysaccharide.

Fig. S4 shows typical FT-IR spectrum of pRCP, which is widely used to analyze the functional groups in polysaccharides. The broad peak at 3429 cm^{-1} was assigned to the O—H stretching vibrations and the peak at 2926 cm^{-1} was the stretching vibrations of the C—H bonds, which are the characteristic absorption peaks of sugars (Wang et al., 2022). Moreover, the peaks at 1620 cm^{-1} and 1418 cm^{-1} were due to the C═O and COO^- stretching vibrations, respectively, which are the feature peaks from uronic acids (Wang et al., 2022). The peak at 1076 cm^{-1} was attributed to the C—O stretching vibrations from the pyranose ring of sugars (Zhang et al., 2022).

The chain conformation of pRCP is illustrated in Fig. S5a, where we can see that the slope value was 0.17 ± 0.01 in the Mw range of 13 kDa to 1,953 kDa, implying that pRCP has a tight, uniform and spherical conformation in 0.1 M $NaNO_3$ solution. Additionally, the molar mass distribution of pRCP is shown in Fig. S5b, and the values of Mw, Mn and polydispersity index (Mw/Mn) are listed in Table S10. A single symmetrical and narrow peak with the polydispersity index of 1.52 indicates that pRCP has a high homogeneity. Moreover, the Mw and Mn values of pRCP were calculated to be 74.86 and 49.19 kDa, respectively (Table S10).

The surface morphology of pRCP was examined by SEM at different magnifications, as illustrated in Fig. S2c. We found that pRCP exhibited smooth surface and porous lamellar structures, suggesting that pRCP might be utilized as encapsulation materials for drug delivery.

3.4. Methylation analysis of pRCP

The glycosidic linkages and molar percentages of sugar residues in pRCP were determined by the methylation analysis (Table S11). The results demonstrate that the molar percentages of *t*-Ara(f), 3-Ara(f), 5-Ara(f) and 2,5-Ara(f) were 23.059, 2.997, 11.156 and 2.446%, respectively. The dominant glycosidic linkage types of pRCP consisted of *t*-Gal(p), 3-Gal(p), 4-Gal(p), 6-Gal(p) and 3,6-Gal(p) with the percentages of 3.477, 4.362, 5.367, 5.782 and 18.344%, respectively (Table S11). Additionally, pRCP was also composed of *t*-Gal(p)-UA and 4-Gal(p)-UA and their percentages were 0.386 and 8.051%, respectively. Thus it can be seen that sugar residues from arabinose and galactose were

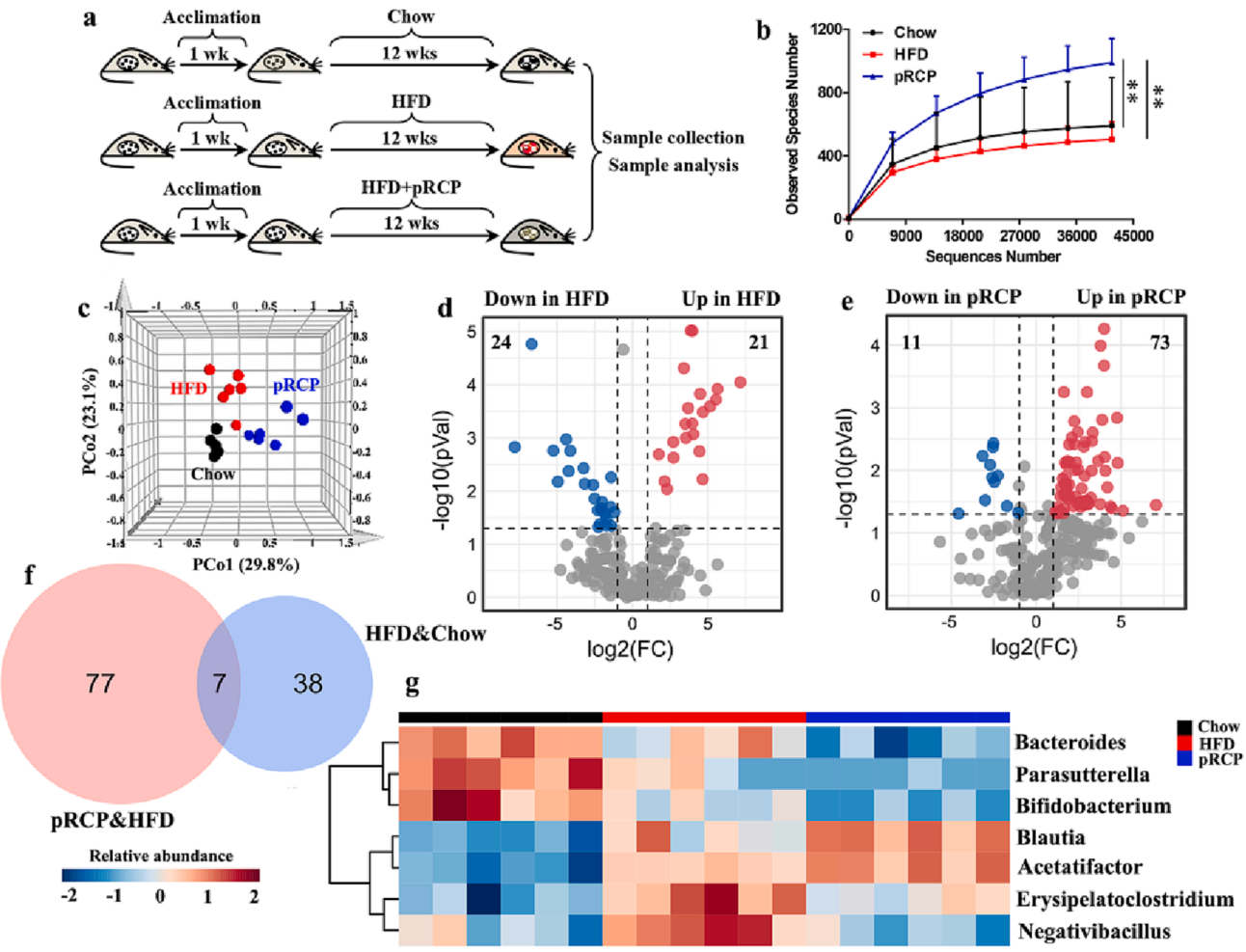

Fig. 2. Raspberry polysaccharide shapes the gut microbiota in HFD-fed mice. (a) After one week acclimatization, mice were given either normal chow (Chow) or high-fat diet (HFD) for 12 weeks; moreover, mice in the third group were fed with HFD plus daily administration of raspberry polysaccharide (pRCP) for 12 weeks; (b) The number of observed species; (c) PCoA analysis based on the gut microbiota at the genus level; (d, e) Volcano plot analysis based on the gut microbiota at the genus level (d) between Chow and HFD groups and (e) between HFD and pRCP groups; (f) Venn diagram identifying the commonly altered gut microbes between Chow and HFD groups and between HFD and pRCP groups; (g) Heatmap showing the commonly altered gut microbes. The statistical difference in the number of observed species between different groups was evaluated by a repeated measure ANOVA. Significant level: **p < 0.01.

highly enriched in pRCP, which is in agreement with monosaccharide composition analysis.

3.5. NMR analysis of pRCP

To further analyze the structure of pRCP, 1D and 2D NMR spectroscopy were carried out in this study. In the ^{1}H NMR spectrum, the chemical shift of pRCP was mainly concentrated in the range of δ3.2–5.4 ppm, and its anomer proton chemical shift was in the range of δ4.4–5.4 ppm (Fig. S6a). The strong signal at δ4.79 ppm was assigned to the solvent proton peak. We identified eight anomer proton signals appeared at δ5.25 ppm, δ4.54 ppm, δ5.10 ppm, δ5.20 ppm, δ4.51 ppm, δ5.17 ppm, δ5.13 ppm and δ5.01 ppm, corresponding to sugar residues A-H, respectively. In the ^{13}C NMR spectrum, the anomeric carbon signals were mainly in the region of δ95-110 ppm (Wang et al., 2022). In this study, six anomalous signals were matched in the anomer carbon region δ99-110 ppm of ^{13}C NMR spectrum (Fig. S6b) and the anomer region of HSQC spectrum (Fig. 1a), namely δ5.25/109.39 ppm, δ4.54/103.37 ppm, δ5.1/107.64 ppm, δ5.2/107.59 ppm, δ4.51/103.59 ppm and δ5.17/109.26 ppm. The sugar residues G and H were not identified in the HSQC spectrum due to excessively low and severely overlapping signals. According to methylation, NMR results and previously reported data (Wang et al., 2018; Wang et al., 2019a; Zhang et al., 2020), the sugar residues A-F were assigned to t-α-Ara*f*(1→, →3,6)-β-Gal*p*(1→, →5)-α-Ara*f*(1→, →4)-α-GalpA(1→, →6)-β-Gal*p*(1 → and → 4)-α-Gal*p* (1→, respectively (Table S12). For residue A, the cross-peak signals were detected at δ5.25/4.22 ppm, δ4.22/3.88 ppm, δ3.88/3.93 ppm and δ3.93/4.14 ppm in the COSY spectrum, indicating that the H2-H5 signals of residue A were at δ4.22 ppm, δ3.88 ppm, δ3.93 ppm and δ4.14 ppm (Fig. 1b; Table S12). Similarly, the identified cross-peaks in the HSQC spectrum at δ4.22/81.52 ppm, δ3.88/67.19 ppm, δ3.93/69.62 ppm and δ4.14/61.46 ppm revealed that the *C*2-C5 resonances were at δ81.52 ppm, δ67.19 ppm, δ69.62 ppm and δ61.46 ppm (Fig. 1a; Table S12). In the same way, the H2-H6 signals and the *C*2-C6 signals of six anomer residues of pRCP were obtained from the COSY and HSQC spectra, as listed in Table S12. For residue B, the chemical shift of C3 to the lower field (δ80.22 ppm) is due to a substitution at this position, which is consistent with the structure of → 3,6)-β-Galp(1 →. For residue D, the signal at δ171.25 ppm belongs to the typical carbon signal of uronic acid C═O and is therefore assigned to C6 of → 4)-α-GalpA(1→ (Table S12).

Next, the HMBC (Fig. 1c) and NOESY (Fig. 1d) spectra were used to analyze the linkage sequences among different sugar residues (Wang et al., 2022) and the detailed assignments were listed in Table S12. In the HMBC spectrum, H1 (δ5.25 ppm) of residue A was correlated to C4 (δ84.01 ppm) of residue D and C3 (δ80.22 ppm) of residue B, suggesting

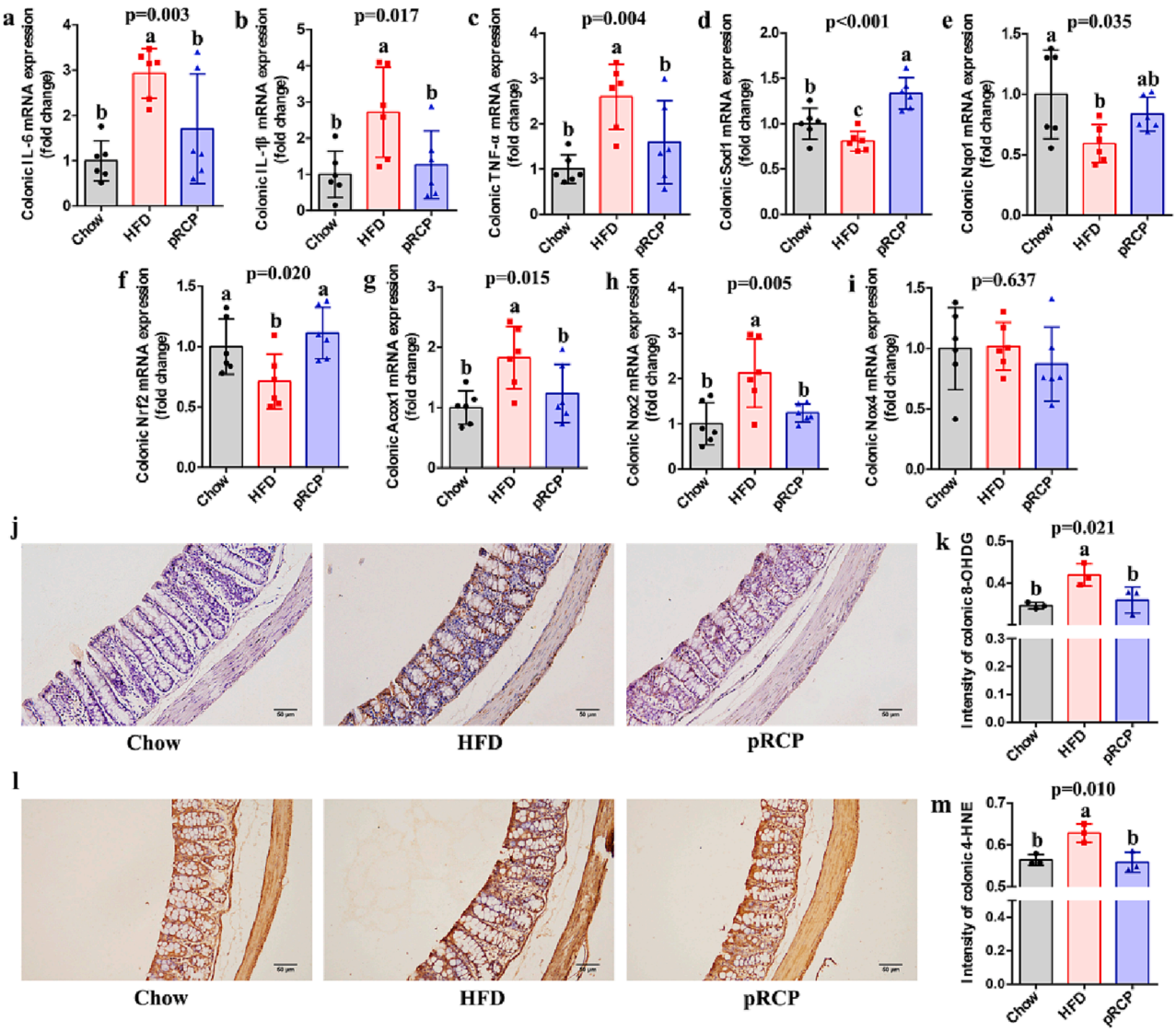

Fig. 3. Raspberry polysaccharide alleviates colonic inflammation and oxidative stress in HFD-fed mice. The mRNA expression levels of (a) IL-6, (b) IL-1β, (c) TNF-α, (d) Sod1, (e) Nqo1, (f) Nrf2, (g) Acox1, (h) Nox2 and (i) Nox 4 in the colon of mice fed with normal chow (Chow), high-fat diet (HFD) or HFD plus daily intake of raspberry polysaccharide (pRCP); (j, k) Immunohistochemical staining of 8-hydroxy-2-deoxyguanosine (8-OHDG) in the colon of mice and the corresponding quantitative data; (l, m) Immunohistochemical staining of 4-hydroxynonenal (4-HNE) in the colon of mice and the corresponding quantitative data. The statistical difference among different groups was analyzed using ANOVA with pairwise comparisons, and different lowercase letters in the figures represent a significant difference.

that residue A is linked to the C4 position of residue D and C3 position of residue B (Fig. 1c; Table S12). Similarly, H1 (δ5.10 ppm) of residue C was connected to C4 (δ84.01 ppm) of residue D and C5 (δ67.03 ppm) of residue C. H1 (δ5.20 ppm) of residue D was coupled to C5 (δ67.03 ppm) of residue C and C4 (δ81.52 ppm) of residue F. The cross-peaks in the HMBC spectrum were also observed between H6 (δ3.66 ppm) of residue E and C1 (δ103.37 ppm) of residue B, H6 (δ3.95 ppm) of residue B and C1 (δ107.64 ppm) of residue C, H1 (δ4.51 ppm) of residue E and C6 (δ69.40 ppm) of residue B, as well as H1 (δ5.17 ppm) of residue F and C3 (δ80.22 ppm) of residue B (Table S12). In addition, the connection between H1 (δ4.54 ppm) and C6 (δ69.40 ppm) of residue B indicates that residue B was self-linked at the C6 position. Subsequently, the NOESY spectrum of pRCP further confirmed the cross-peaks (Fig. 1d): H1 of residue A coupled with H4 of residue D and H3 of residue B; H1 of residue B with H6 of residues B and E; H1 of residue C with H5 of residue C and H4 of residue D; H1 of residue D with H4 of residue F; H1 of residue E with H6 of residues B and E. Based on the above results, it can be speculated that the structure of pRCP consisted of → 3,6)-β-Gal*p*(1 → and → 5)-α-Ara*f*(1 → as the main chain, and the side chain was mainly composed of α-Ara*f*(1 → linked to the C3 position of → 3,6)-β-Gal*p*(1→, as shown in Fig. 1e.

3.6. pRCP modifies the gut microbiota in HFD-fed mice

To examine the effect of pRCP treatment on the gut microbiota of HFD-fed mice, we fed mice with normal chow, HFD or HFD plus daily intake of pRCP for 12 weeks, as illustrated in Fig. 2a. The results show that mice fed with HFD had a slight but not significant decrease in the number of observed species than mice fed with normal chow, but this number can be significantly increased in HFD-fed mice after pRCP treatment (Fig. 2b). Reduced gut microbial diversity has been associated with multiple human diseases (Mosca et al., 2016; Kriss et al., 2018) and healthy diets can recover this undesirable effect (Amamoto et al., 2022). Plant-derived polysaccharides have also been reported to increase the gut microbial diversity (Hao et al., 2022). Herein our results suggest that pRCP could be an alternative prebiotics for enhancing the gut microbial

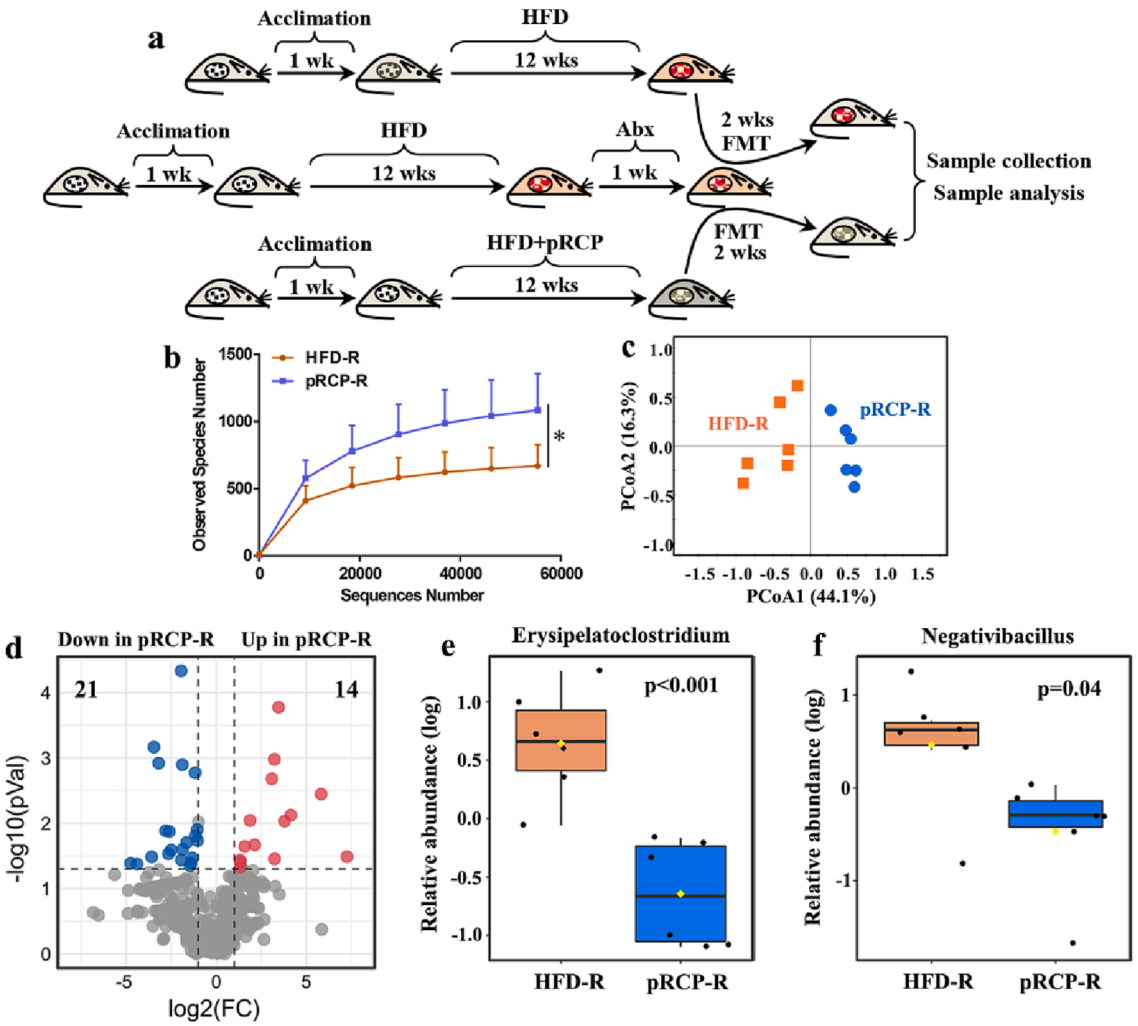

Fig. 4. FMT altered the gut microbiota in HFD-fed mice. (a) After one week acclimatization, mice were given high-fat diet (HFD) for 12 weeks and then received the faecal microbiota from mice fed with either HFD (HFD-R) or HFD plus raspberry polysaccharide (pRCP-R) for 2 weeks; (b) The number of observed species; (c) PCoA analysis based on the gut microbiota at the genus level; (d) Volcano plot analysis based on the gut microbiota at the genus level between HFD-R and pRCP-R mice; (e, f) The relative abundances of *Erysipelatoclostridium* and *Negativibacillus* in HFD-R and pRCP-R mice. The statistical difference between two groups was evaluated by two-tailed unpaired student's T test. The statistical difference in the number of observed species between different groups was evaluated by a repeated measure ANOVA. Significant level: *p < 0.05.

diversity.

Furthermore, we analyzed the impact of pRCP on the gut microbiota at the genus level. The PCoA result reveals that the pRCP group was clearly separated from the chow and HFD groups (Fig. 2c), indicating that pRCP supplement shaped the gut microbial pattern of HFD-fed mice. The volcano plot analysis was performed to identify key gut microbes that significantly altered between the HFD and chow groups (Fig. 2d) and between the pRCP and HFD groups (Fig. 2e), and these identified gut microbes were presented by heatmaps in Figures S7 and S8, respectively. Then, the Venn diagram was used to show the shared gut microbes, where we found that there were 7 gut microbes that were commonly altered in mice after HFD and pRCP treatments (Fig. 2f) and presented in a heatmap (Fig. 2g). The results show that the relative abundances of *Bacteroides, Parasutterella* and *Bifidobacterium* were significantly reduced in HFD-fed mice compared with mice fed with normal chow and further decreased after pRCP treatment (Fig. 2g). However, opposite results were observed in *Blautia* and *Acetatifactor*. Relative to mice fed with normal chow, of note, the relative abundances of *Erysipelatoclostridium* and *Negativibacillus* were significantly enriched in HFD-fed mice, but their abundances were suppressed after pRCP treatment (Fig. 2g). *Erysipelatoclostridium* and *Negativibacillus* have been regarded as harmful bacteria. For example, Zakham et al. (2019) reported that infection with *Erysipelatoclostridium* can lead to septic pseudoarthrosis in a female young patient. *Erysipelatoclostridium ramosum* was also identified as a key mediator of fluoride-induced obesity in mice, which may be a potential target for the prevention and treatment of obesity (Chen et al., 2022). Moreover, Cai et al. (2022) found that gut bacteria *Erysipelatoclostridium* might be a possible pathogen in radiation-induced intestinal injury. The abundance of *Negativibacillus* has been found to be higher in the cecal content of mice with obesity-associated metabolic syndrome (Wang et al., 2019b). In addition, *Negativibacillus* might be potential pathogenic bacteria for gut dysbiosis (Tang et al., 2021) and pediatric Crohn's disease (Wang et al., 2021). Therefore, pRCP could be used as a promising prebiotics to increase the gut microbial diversity and decrease the abundances of harmful bacteria in HFD-fed mice.

3.7. pRCP alleviates inflammation and oxidative stress in the colon of HFD-fed mice

In this study, we found that body weight was significantly increased in HFD-fed mice relative to normal chow-fed mice, but markedly reduced after pRCP treatment (Fig. S9). This finding suggests that pRCP may have a body weight-lowering effect. Intake of HFD not only affected

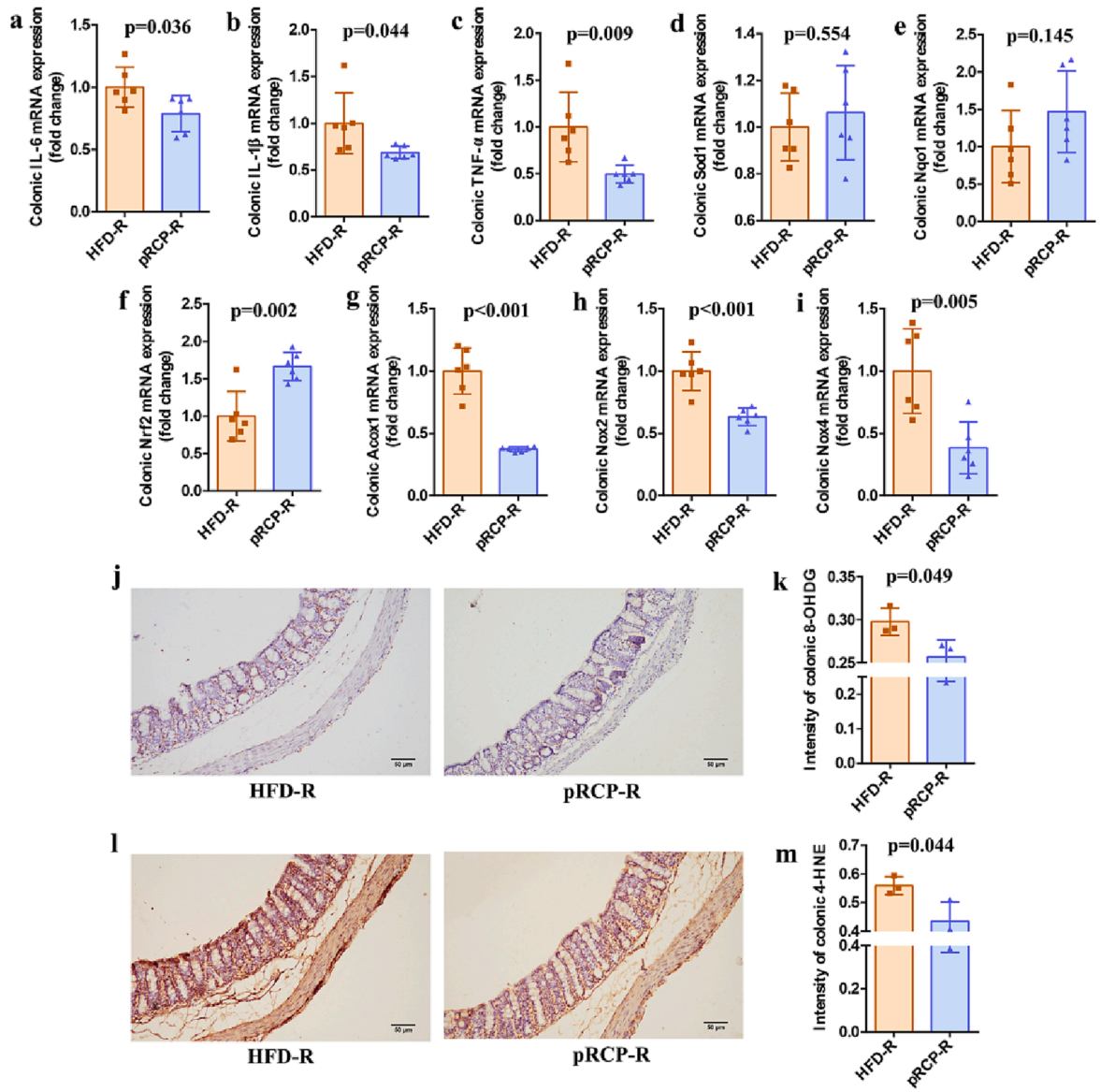

Fig. 5. FMT reduces colonic inflammation and oxidative stress in HFD-fed mice. The mRNA expression levels of (a) IL-6, (b) IL-1β, (c) TNF-α, (d) Sod1, (e) Nqo1, (f) Nrf2, (g) Acox1, (h) Nox2 and (i) Nox 4 in the colon of high-fat diet (HFD)-fed mice received the faecal microbiota from mice fed with either HFD (HFD-R) or HFD plus raspberry polysaccharide (pRCP-R); (j, k) Immunohistochemical staining of 8-hydroxy-2-deoxyguanosine (8-OHDG) in the colon of HFD-R and pRCP-R mice and the corresponding quantitative data; (l, m) Immunohistochemical staining of 4-hydroxynonenal (4-HNE) in the colon of HFD-R and pRCP-R mice and the corresponding quantitative data. The statistical difference between two groups was evaluated by two-tailed unpaired student's T test.

body weight and the gut microbiota (Zhang & Yang, 2016) but also promoted inflammation and oxidative stress in the colon (Li et al., 2019). Therefore, to investigate the effect of pRCP treatment on inflammation and oxidative stress, we analyzed several inflammatory cytokines and oxidative stress indicators in the colon of HFD-fed mice after pRCP supplement. The results reveal that HFD drastically increased the expression levels of IL-6 (Fig. 3a), IL-1β (Fig. 3b) and TNF-α (Fig. 3c) in the colon of mice, but their levels were significantly suppressed after pRCP treatment. Compared with mice fed with normal chow, the colonic levels of antioxidative indicators were significantly reduced in HFD-fed mice including Sod1 (Fig. 3d), Nqo1 (Fig. 3e) and Nrf2 (Fig. 3f), whereas pRCP supplement can recover their levels to the normal level. Also, the mRNA levels of pro-oxidative indexes including Acox1 (Fig. 3g) and Nox2 (Fig. 3h) were notably increased in the colon of mice after HFD feeding, but significantly reduced in HFD-fed mice after pRCP treatment. For Nox4, a slight but not significant decrease was obtained in the pRCP group relative to other two groups (Fig. 3i). Afterward, we measured the protein levels of 8-hydroxy-2-deoxyguanosine (8-OHDG), a biomarker of DNA oxidative damage, and 4-hydroxynonenal (4-HNE), a biomarker of oxidative stress, in the colon of mice by using immunohistochemical staining, as shown in Fig. 3j and l, respectively. The quantitative results reveal that the intensities of both 8-OHDG (Fig. 3k) and 4-HNE (Fig. 3m) positive staining were significantly higher in the colon of mice fed with HFD and recovered to the normal level after pRCP treatment. Collectively, our results suggest that pRCP has the ability to alleviate HFD-induced colonic inflammation and oxidative stress in mice.

3.8. pRCP-modified gut microbiota exhibits a protective effect on inflammation and oxidative stress in the colon of HFD-fed mice

To verify the causal role of the gut microbiota in the protective effect on colonic disorders caused by HFD, the faecal microbiota from mice fed with either HFD or pRCP was transferred to HFD-fed recipient mice

(HFD-R and pRCP-R) for 2 weeks (Fig. 4a). Compared with HFD-R mice, the number of observed species was significantly higher in pRCP-R mice (Fig. 4b), suggesting that higher gut microbial diversity can be transferred to HFD-fed recipient mice. The PCoA result based on the gut microbiome shows that the gut microbial pattern of pRCP-R mice was clearly separated from that of HFD-R mice at the genus level (Fig. 4c). Subsequently, volcano plot analysis was carried out to identify significantly altered gut microbes between HFD-R and pRCP-R mice (Fig. 4d). The identified microbes were presented as a heatmap in Fig. S10, where we found that the relative abundances of *Erysipelatoclostridium* (Fig. 4e) and *Negativibacillus* (Fig. 4f) were significantly lower in pRCP-R mice than HFD-R mice. These findings indicate that the characteristic of the gut microbiota modified by pRCP were partly transferred to recipient mice as indicated by reduced *Erysipelatoclostridium* and *Negativibacillus*.

Interestingly, the expression levels of inflammatory factors were significantly reduced in the colon of pRCP-R mice relative to HFD-R mice including IL-6 (Fig. 5a), IL-1β (Fig. 5b) and TNF-α (Fig. 5c). Compared with HFD-R mice, we observed slightly but not significantly higher levels of Sod1 (Fig. 5d) and Nqo1 (Fig. 5e) in the colon of pRCP-R mice. Yet, a significantly increased Nrf2 level was obtained in pRCP-R mice than HFD-R mice (Fig. 5f). In addition, pRCP-R mice had significantly lower levels of Acox1 (Fig. 5g), Nox2 (Fig. 5h) and Nox4 (Fig. 5i) in the colon than HFD-R mice. These results were further confirmed from immunohistochemical staining as indicated by significant reductions in the intensities of 8-OHDG (Fig. 5j and k) and 4-HNE (Fig. 5l and m) positive staining in the colon of pRCP-R mice compared with HFD-R mice. Hence, our results indicate that colonic inflammation and oxidative stress in HFD-fed mice can be inhibited by pRCP-modified gut microbiota.

4. Conclusion

In this study, we optimized the extraction procedure of polysaccharides from unripe raspberry fruits via a three steps methodology and characterized the detailed structure of the main fraction of polysaccharides (pRCP). We reported that pRCP is an acidic heteropolysaccharide consisted of fucose, arabinose, galactose, glucose, xylose, mannose, galacturonic acid and glucuronic acid with many linkages, and its main chain is made up of → 3,6)-*β*-Gal*p*(1 → and → 5)-*α*-Ara*f*(1 →. pRCP displays a high homogeneity, and its Mw and Mn are 74.864 and 49.187 kDa, respectively. Besides, we found that pRCP treatment can increase the gut microbial diversity and decrease the abundances of harmful bacteria in HFD-fed mice. Both pRCP intake and FMT from pRCP-treated mice alleviated HFD-induced inflammation and oxidative stress in the colon of mice. Thus, pRCP could be used as a promising prebiotic to improve gut dysbiosis caused by HFD in the future. However, several aspects need to be noted: First, immature raspberry fruits are not recommended as edible fruits due to bitter taste, but could be a source of functional polysaccharides; Second, these beneficial effects proposed herein may not be achieved by directly consuming unripe raspberry fruits because of a low content of pRCP; Lastly, it is of great importance to produce more pRCP from unripe raspberry fruits via optimizing extraction processes and selecting preferable varieties and harvest time.

CRediT authorship contribution statement

Hanqi Luo: Formal analysis, Methodology, Investigation, Visualization, Writing – original draft, Writing – review & editing. **Na Ying:** Methodology, Investigation, Writing – original draft, Writing – review & editing. **Qihui Zhao:** Investigation, Writing – review & editing, Visualization. **Junli Chen:** Investigation, Writing – review & editing. **Hangying Xu:** Investigation, Writing – review & editing. **Wu Jiang:** Investigation, Writing – review & editing. **Yaozong Wu:** Visualization, Writing – review & editing. **Yinliang Wu:** Writing – review & editing. **Hongchang Gao:** Supervision, Project administration, Writing – review & editing. **Hong Zheng:** Conceptualization, Data curation, Supervision, Project administration, Funding acquisition, Writing – original draft, Writing – review & editing.

Declaration of Competing Interest

The authors declare that they have no known competing financial interests or personal relationships that could have appeared to influence the work reported in this paper.

Data availability

Data will be made available on request.

Acknowledgments

This study was supported by the National Natural Science Foundation of China (No.: 22074106). We are grateful for the assistance from the Scientific Research Center of Wenzhou Medical University. Images used in the graphical abstract were obtained from BioRender.

Appendix A. Supplementary data

Supplementary data to this article can be found online at https://doi.org/10.1016/j.foodchem.2023.136152.

References

Amamoto, R., Shimamoto, K., Suwa, T., Park, S., Matsumoto, H., Shimizu, K., et al. (2022). Relationships between dietary diversity and gut microbial diversity in the elderly. *Beneficial Microbes*, 1–12.

Burton-Freeman, B. M., Sandhu, A. K., & Edirisinghe, I. (2016). Red raspberries and their bioactive polyphenols: Cardiometabolic and neuronal health links. *Advances in Nutrition, 7*(1), 44–65.

Cai, S., Yang, Y., Kong, Y., Guo, Q., Xu, Y., Xing, P., et al. (2022). Gut bacteria *Erysipelatoclostridium* and its related metabolite ptilosteroid A could predict radiation-induced intestinal injury. *Frontiers in Public Health, 10*, Article 862598.

Chen, F., & Huang, G. (2018). Preparation and immunological activity of polysaccharides and their derivatives. *International Journal of Biological Macromolecules, 112*, 211–216.

Chen, G., Peng, Y., Huang, Y., Xie, M., Dai, Z., Cai, H., et al. (2022). Fluoride induced leaky gut and bloom of *Erysipelatoclostridium ramosum* mediate the exacerbation of obesity in high-fat-diet fed mice. *Journal of Advanced Research, 2022*. https://doi.org/10.1016/j.jare.2022.10.010

Chen, Y., Wang, Y., Xu, L., Jia, Y., Xue, Z., Zhang, M., et al. (2020). Ultrasound-assisted modified pectin from unripe fruit pomace of raspberry (*Rubus chingii* Hu): Structural characterization and antioxidant activities. *LWT, 134*, Article 110007.

Hancock, C. R., Han, D. H., Chen, M., Terada, S., Yasuda, T., Wright, D. C., et al. (2008). High-fat diets cause insulin resistance despite an increase in muscle mitochondria. *Proceedings of the National Academy of Sciences, 105*(22), 7815–7820.

Hansen, P., Mladenović, N., Brimberg, J., & Pérez, J. A. M. (2019). Variable neighborhood search. In *Handbook of metaheuristics* (pp. 57–97). Cham: Springer.

Hao, W., Chen, Z., Yuan, Q., Ma, M., Gao, C., Zhou, Y., et al. (2022). Ginger polysaccharides relieve ulcerative colitis via maintaining intestinal barrier integrity and gut microbiota modulation. *International Journal of Biological Macromolecules, 219*, 730–739.

Kim, J. B., & Carpita, N. C. (1992). Changes in esterification of the uronic acid groups of cell wall polysaccharides during elongation of maize coleoptiles. *Plant Physiology, 98*, 646–653.

Klewicka, E., Sójka, M., Ścieszka, S., Klewicki, R., Milczarek, A., Lipińska, L., et al. (2020). The antimycotic effect of ellagitannins from raspberry (*Rubus idaeus* L.) on Alternaria alternata ŁOCK 0409. *European Food Research and Technology, 246*(7), 1341–1349.

Kriss, M., Hazleton, K. Z., Nusbacher, N. M., Martin, C. G., & Lozupone, C. A. (2018). Low diversity gut microbiota dysbiosis: Drivers, functional implications and recovery. *Current Opinion in Microbiology, 44*, 34–40.

Li, X., Wei, X., Sun, Y., Du, J., Li, X., Xun, Z., et al. (2019). High-fat diet promotes experimental colitis by inducing oxidative stress in the colon. *American Journal of Physiology-Gastrointestinal and Liver. Physiology, 317*(4), G453–G462.

Lian, C. Y., Zhai, Z. Z., Li, Z. F., & Wang, L. (2020). High fat diet-triggered non-alcoholic fatty liver disease: A review of proposed mechanisms. *Chemico-Biological Interactions, 330*, Article 109199.

Lu, Q., Li, R., Yang, Y., Zhang, Y., Zhao, Q., & Li, J. (2022). Ingredients with anti-inflammatory effect from medicine food homology plants. *Food Chemistry, 368*, Article 130610.

Mazur, S. P., Nes, A., Wold, A. B., Remberg, S. F., & Aaby, K. (2014). Quality and chemical composition of ten red raspberry (*Rubus idaeus* L.) genotypes during three harvest seasons. *Food Chemistry, 160*, 233–240.

Mosca, A., Leclerc, M., & Hugot, J. P. (2016). Gut microbiota diversity and human diseases: Should we reintroduce key predators in our ecosystem? *Frontiers in Microbiology, 7*, 455.

Noratto, G. D., Chew, B. P., & Atienza, L. M. (2017). Red raspberry (*Rubus idaeus* L.) intake decreases oxidative stress in obese diabetic (*db/db*) mice. *Food Chemistry, 227*, 305–314.

Ravussin, E., & Tataranni, P. A. (1997). Dietary fat and human obesity. *Journal of the American Dietetic Association, 97*(7), S42–S46.

Rohr, M. W., Narasimhulu, C. A., Rudeski-Rohr, T. A., & Parthasarathy, S. (2020). Negative effects of a high-fat diet on intestinal permeability: A review. *Advances in Nutrition, 11*(1), 77–91.

Salvador, L. D., Suganuma, T., Kitahara, K., Tanoue, H., & Ichiki, M. (2000). Monosaccharide composition of sweetpotato fiber and cell wall polysaccharides from sweetpotato, cassava, and potato analyzed by the high-performance anion exchange chromatography with pulsed amperometric detection method. *Journal of Agricultural and Food Chemistry, 48*(8), 3448–3454.

Staszowska-Karkut, M., & Materska, M. (2020). Phenolic composition, mineral content, and beneficial bioactivities of leaf extracts from black currant (*Ribes nigrum* L.), raspberry (*Rubus idaeus*), and aronia *(Aronia melanocarpa*). *Nutrients, 12*(2), 463.

Su, X., Zhao, M., Fu, X., Ma, X., Xu, W., & Hu, S. (2021b). Immunomodulatory activity of purified polysaccharides from *Rubus chingii* Hu fruits in lymphocytes and its molecular mechanisms. *Journal of Functional Foods, 87*, Article 104785.

Su, Y., Li, J., Wu, L., & Kuang, H. (2021a). Polysaccharides from TCM herbs exhibit potent anti-obesity effect by mediating the community structure of gut microbiota. *Pharmazie, 76*(10), 473–479.

Szymanowska, U., Baraniak, B., & Bogucka-Kocka, A. (2018). Antioxidant, anti-inflammatory, and postulated cytotoxic activity of phenolic and anthocyanin-rich fractions from polana raspberry (*Rubus idaeus* L.) fruit and juice-In vitro study. *Molecules, 23*(7), 1812.

Tang, S., Zhong, R., Yin, C., Su, D., Xie, J., Chen, L., et al. (2021). Exposure to high aerial ammonia causes hindgut dysbiotic microbiota and alterations of microbiota-derived metabolites in growing pigs. *Frontiers in Nutrition, 8*, Article 689818.

Ummat, V., Sivagnanam, S. P., Rajauria, G., O'Donnell, C., & Tiwari, B. K. (2021). Advances in pre-treatment techniques and green extraction technologies for bioactives from seaweeds. *Trends in Food Science & Technology, 110*, 90–106.

Wang, B. H., Cao, J. J., Zhang, B., & Chen, H. Q. (2019a). Structural characterization, physicochemical properties and α-glucosidase inhibitory activity of polysaccharide from the fruits of wax apple. *Carbohydrate Polymers, 211*, 227–236.

Wang, L., Liu, H. M., Xie, A. J., Wang, X. D., Zhu, C. Y., & Qin, G. Y. (2018). Chinese quince (*Chaenomeles sinensis*) seed gum: Structural characterization. *Food Hydrocolloids, 75*, 237–245.

Wang, L., Zhao, Z., Zhao, H., Liu, M., Lin, C., Li, L., et al. (2022). Pectin polysaccharide from *Flos Magnoliae* (Xin Yi, *Magnolia biondii* Pamp. flower buds): Hot-compressed water extraction, purification and partial structural characterization. *Food Hydrocolloids, 122*, Article 107061.

Wang, W., Pan, Y., Wang, L., Zhou, H., Song, G., Wang, Y., et al. (2019b). Optimal dietary ferulic acid for suppressing the obesity-related disorders in leptin-deficient obese C57BL/6J-ob/ob mice. *Journal of Agricultural and Food Chemistry, 67*(15), 4250–4258.

Wang, Y., Gao, X., Zhang, X., Xiao, F., Hu, H., Li, X., et al. (2021). Microbial and metabolic features associated with outcome of infliximab therapy in pediatric Crohn's disease. *Gut Microbes, 13*(1), 1865708.

Xu, Y., Liu, N., Fu, X., Wang, L., Yang, Y., Ren, Y., et al. (2019). Structural characteristics, biological, rheological and thermal properties of the polysaccharide and the degraded polysaccharide from raspberry fruits. *International Journal of Biological Macromolecules, 132*, 109–118.

Yang, Y., Yin, X., Zhang, D., Lu, J., & Wang, X. (2022). Isolation, structural characterization and macrophage activation activity of an acidic polysaccharide from raspberry pulp. *Molecules, 27*(5), 1674.

Yu, Z., Liu, L., Xu, Y., Wang, L., Teng, X., Li, X., et al. (2015). Characterization and biological activities of a novel polysaccharide isolated from raspberry (*Rubus idaeus* L.) fruits. *Carbohydrate Polymers, 132*, 180–186.

Zakham, F., Pillonel, T., Brunel, A. S., Zambelli, P. Y., Greub, G., Croxatto, A., et al. (2019). Molecular diagnosis and enrichment culture identified a septic pseudoarthrosis due to an infection with *Erysipelatoclostridium* ramosum. *International Journal of Infectious Diseases, 81*, 167–169.

Zhang, H., Li, C., Ding, J., Lai, P. F., Xia, Y., & Ai, L. (2020). Structural features and emulsifying stability of a highly branched arabinogalactan from immature peach (Prunus persica) exudates. *Food Hydrocolloids, 104*, Article 105721.

Zhang, M., & Yang, X. J. (2016). Effects of a high fat diet on intestinal microbiota and gastrointestinal diseases. *World Journal of Gastroenterology, 22*(40), 8905.

Zhang, N. N., Ma, H., Zhang, Z. F., Zhang, W. N., Chen, L., Pan, W. J., et al. (2022). Characterization and immunomodulatory effect of an alkali-extracted galactomannan from morchella esculenta. *Carbohydrate Polymers, 278*, Article 118960.

Zhou, W., Chen, G., Chen, D., Ye, H., & Zeng, X. (2020). The antidiabetic effect and potential mechanisms of natural polysaccharides based on the regulation of gut microbiota. *Journal of Functional Foods, 75*, Article 104222.